Polymer 51 (2010) 5744–5755

Contents lists available at ScienceDirect

Polymer

journal homepage: www.elsevier.com/locate/polymer

Effect of nanowhisker-modified zeolites on mechanical and thermal properties of poly(vinyl acetate) composites with pure-silica MFI

Jung-Hyun Lee, Pedro Zapata, Sunho Choi, J. Carson Meredith*

School of Chemical and Biomolecular Engineering, Georgia Institute of Technology, 311 Ferst Drive NW, Atlanta, GA 30332, USA

ARTICLE INFO

Article history:
Received 14 July 2010
Received in revised form
25 September 2010
Accepted 28 September 2010
Available online 7 October 2010

Keywords:
Polymers
Composites
Nanostructures

ABSTRACT

The effect of nanoscale surface morphology of pure-silica MFI zeolite on the interfacial, mechanical, and thermal properties of pure-silica MFI zeolite/poly(vinyl acetate) (PVAc) composites was investigated under different annealing conditions. $Mg(OH)_2$ inorganic whisker- or asperity-like nanostructures were achieved on MFI nano- and micro-particle surfaces via Grignard or solvothermal treatment. The creation of nano-roughness on the MFI surface promoted compatibility between the zeolite and the polymer matrix, resulting in void-free interfaces. PVAc composites containing surface-modified particles showed increased tensile strength and elongation at break as compared with composites containing unmodified zeolite. Surface modification of the microparticles exhibited interfacial and mechanical enhancement over a wider range of annealing temperatures than nanoparticles. Differential scanning calorimetry revealed that surface treatment of MFI resulted in broader glass transitions compared to composites containing unmodified MFI. This is explained by improved interfacial adhesion and associated slower chain relaxation dynamics. Furthermore, X-ray diffraction demonstrated that enhanced adhesive interactions between the PVAc and the MFI surface are associated with surface-induced orientation of the MFI particles within the polymer matrix. The optimal surface morphology, associated with the most enhanced mechanical and thermal properties of composites, was produced with the solvothermal method.

© 2010 Elsevier Ltd. All rights reserved.

1. Introduction

The incorporation of inorganic zeolite materials into polymer matrices has been exploited intensively in order to improve thermal [1], optical [2,3], electrical [4,5], catalytic [6,7], and transport properties [8]. In particular, in the field of gas separation and liquid pervaporation, a general trade-off exists between permeability and selectivity for polymer-only membranes and hence limits applications of polymeric materials to energy-saving separation [9]. Mixed matrix materials comprised of highly selective zeolites embedded in a polymer matrix have the potential to provide membranes with dramatically improved selectivity [10,11], relative to polymer-only membranes. However, many studies have illustrated the difficulties of achieving defect-free and hence highly-performing zeolite-based polymer composite materials by physically mixing zeolite particles with polymer solutions. These difficulties arise in part from limited intrinsic compatibility between the zeolite and the polymer, and interfacial voids often exist at the zeolite–polymer interfaces [12–15]. Hence, many studies of zeolite–polymer composite materials have focused primarily on interfacial tailoring to promote adhesion between the inorganic and polymer species in order to minimize interfacial defects. Intensive efforts to yield defect-free composite materials have been carried out using silane coupling agents, integral chain linkers, and polymer coatings on the molecular sieve surfaces [12,16–18]. Unfortunately, although these organic functionalization routes reduce interfacial voids, they are not able to eliminate defects completely. In addition, use of coupling agents is usually limited to a specific polymer–filler pair depending on the chemistry of the polymeric materials. Recently, a new approach for zeolite surface modification was proposed to achieve a defect-free composite. Grignard or solvothermal treatment was employed to create $Mg(OH)_2$ inorganic whisker or asperity nanostructures on the zeolite surface [15,19,20]. The highly roughened zeolite surfaces are thought to promote adhesion at the polymer–particle interface via thermodynamically-induced adsorption and physical entanglement of polymer chains in the whisker structures by minimizing the entropy penalty, and yielded defect-free composite membranes with enhanced gas separation efficiency [15].

The nature of the particle–polymer interface strongly influences the macroscopic response, and improved properties of composites

* Corresponding author. Tel.: +1 404 385 2151; fax: +1 404 894 2866.
E-mail address: carson.meredith@chbe.gatech.edu (J.C. Meredith).

0032-3861/$ – see front matter © 2010 Elsevier Ltd. All rights reserved.
doi:10.1016/j.polymer.2010.09.071

are known to be related to the modification of the structure and dynamics of the polymer due to altered interaction with the filler surface [21–23]. Furthermore, the polymer properties can be affected profoundly by the thermo-mechanical history during membrane fabrication [24]. Hence, questions arise as to how the presence of inorganic nanostructures on the zeolite surface influences the interfacial and associate properties of the composites depending on thermal history. Knowledge of the roughening effect of the particle surfaces on interfacial and physical properties of composites would allow better design of surface treatments.

This paper reports on the effects of inorganic nanostructures on MFI zeolite surfaces on the interfacial, mechanical and thermal properties of zeolite-loaded polymer composites. Poly(vinyl acetate) (PVAc) and pure-silica MFI were selected as a model polymer and filler matrix, respectively. PVAc, an amorphous and thermoplastic polymer, has attracted interest due to applications in gas separation membranes, as well as adhesives, textiles and resin emulsifiers [13–15,25]. Pure-silica MFI zeolite (also known as ZSM-5: Zeolite Socony Mobil-Five) comprises SiO_2 tetrahedra having pore size between 5.1 and 5.6 Å with an interconnected pore structure that consist of sinusoidal, straight, tortuous pore channels [26]. MFI zeolite has been commonly used in gas separation and catalysis applications due to its intrinsic molecular-sieving properties [19,20,26]. Although MFI is regarded as the most hydrophobic among other types of aluminosilicate zeolites, it is likely that the silanols on the MFI surfaces may interact favorably with the carbonyl groups on PVAc [26]. Inorganic nanoscale asperities on the MFI surfaces were obtained by Grignard or solvothermal treatments of MFI particles. PVAc composites containing unmodified and surface-modified MFI particles were prepared by solvent casting. The structural, mechanical, and thermal properties of the composite films were investigated as a function of MFI loading, size and surface treatment, as well as film annealing temperatures. Scanning electron microscopy (SEM) was used to examine the surface morphologies of the particles, as well as the interfacial morphology and particle dispersion in the resultant composite films. High-throughput mechanical characterization (HTMECH) and differential scanning calorimetry (DSC) were employed to characterize mechanical and thermal behavior of the composite films, respectively. X-ray diffraction (XRD) was conducted to examine the structural properties of the composite films. The influence of zeolite nanostructured surface morphology on properties of the composites is discussed. Based on the results, an optimal surface modification protocol was proposed.

2. Experimental section

2.1. Materials

The following chemicals were used as received: poly(vinyl acetate) (PVAc, $M_w = 500{,}000$ g/mol, Sigma–Aldrich), tetraethylorthosilicate (TEOS, 98% Sigma–Aldrich), tetrapropylammonium hydroxide (TPAOH, 40% w/w aqueous solution, Alfa Aesar), tetrapropylammonium bromide (TPABr, 98%, Sigma–Aldrich), ethylenediamine (EDA, 99%, Sigma–Aldrich), methylmagnesium bromide (3 M in ether, Sigma–Aldrich), 2-propanol (Sigma–Aldrich), dichloromethane (DCM, 99.5%, Sigma–Aldrich), toluene (99.8%, Sigma–Aldrich), magnesium sulfate heptahydrate (Acros) and sodium chloride (NaCl, Fisher Scientific).

2.2. Synthesis of pure-silica MFI crystals

Pure-silica MFI nanoparticles (nMFIs) were synthesized hydrothermally from TEOS/TPAOH/water solutions. The solution with molar ratio of 1 TEOS/0.24 TPAOH/360 H_2O was stirred at room temperature for 24 h and hydrothermally crystallized at 150 °C for 4 days. Large MFI microparticles (μMFIs) were also prepared using the method described in the literature [19]. The solution with molar ratio of 1 TEOS/0.1 TPABr/0.1 NaOH/98 H_2O was aged at 50 °C for 7 days and crystallized at 120 °C for 2 days. The synthesized zeolite particles were then washed with DI water via at least five centrifugation cycles, followed by drying at 80 °C. The particles were calcined at 550 °C for 8 h in air.

2.3. Surface modification of MFI crystals

2.3.1. Grignard treatment (GT)

Grignard treatment was performed after seeding the zeolite surfaces with NaCl. 0.5 g of MFI particles was dispersed in 3 M aqueous NaCl solution. The suspension was filtered using a microfiltration membrane with 0.1 μm pores. The collected particles were then dried at 80 °C for 12 h to remove residual water. The NaCl seeded particles were placed in round bottom flask, followed by the addition of 8 ml of toluene. After purging the flask with nitrogen 1.5 ml of 3 M CH_3MgBr in ether was added using transfer needles. The suspension was sonicated at 20 kHz for 4 h and then stirred at room temperature under nitrogen for 12 h. 2-propanol was added drop-wise to quench the Grignard reagent and the mixture was centrifuged to collect the particles. To remove residual solvents, the particles were washed with 2-propnaol several times. After that, 40 ml of DI water was added to the particles and the mixture was sonicated at 20 kHz for 2 h. The particles were washed with DI water via several cycles of centrifugation and dispersion, followed by drying at 80 °C.

2.3.2. Solvothermal treatment (ST)

The deposition of $Mg(OH)_2$ was performed in the solvent mixture of EDA and a $MgSO_4$ aqueous solution at high temperature. 0.2 g of zeolites was dispersed in 10 ml of EDA by sonication, followed by the drop-wise addition of 1 ml of 1 M aqueous $MgSO_4$ solution under vigorous stirring. After further stirring for 1 h, the mixture was transferred to Teflon-lined autoclave and solvothermal treatment was performed at 160 °C in the oven for 12 h. The particles were washed with DI water via several centrifugation cycles and dried at 80 °C. The amount of $Mg(OH)_2$ in final products was controlled by adjusting $MgSO_4$ concentration in the aqueous solution. The detailed procedure was described in the literature [19].

2.3.3. MFI/PVAc composite film preparation

Unmodified and surface-treated MFI zeolites were dried in a vacuum oven at 140 °C for 24 h. The proper amounts of dried particles (to form 1, 2.5, 5, and 10 vol.% MFI loaded films) were dispersed in DCM by stirring for 24 h, followed by bath and horn type sonication at 42 kHz for 20 min and at 20 kHz for 1 min, respectively. Sonication procedures were repeated at least 3 times to ensure a uniform dispersion of zeolite particles in the solvent. The desired amount of dried PVAc was added to the zeolite suspensions, and then the mixtures were agitated using a rotational shaker for 48 h. The composite films were prepared by casting the solution mixtures with a blade on OTS (Octadecyltrichlorosilane)-treated glass substrates, and slowly dried under a solvent (DCM) saturated environment for 24 h. The films were subsequently dried at room temperature for 7 days, and free standing films were obtained by carefully peeling films from the glass using a razor. Finally, composite films were annealed in a vacuum oven at either 20, 40, or 100 °C for 24 h. All samples were slowly cooled down to room temperature at ~6 °C/h cooling rate. The thickness at various positions on the films was measured by a micrometer (Mitutoyo Corp., model C112CEB). For each film, 25 measurements were

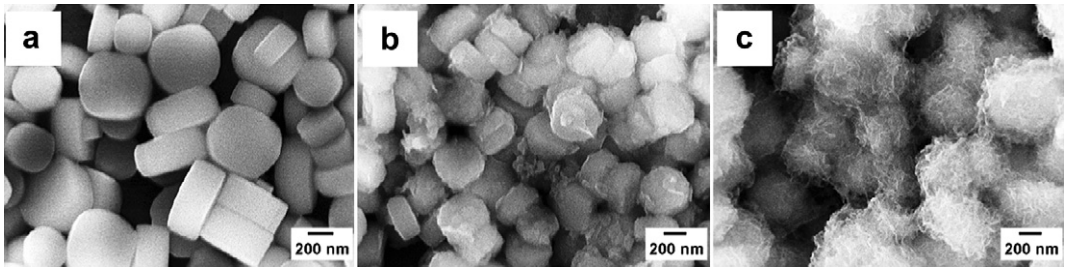

Fig. 1. MFI nanoparticles (nMFIs); (a) untreated (UN), (b) Grignard-treated (GT), and (c) solvothermally-treated (ST).

performed within 2.5 × 2.0 cm^2 area of the film, and the average thinness was obtained. All the films used in this work had an average thickness of 110 ± 3 μm.

2.4. Characterization

2.4.1. MFI zeolite particles

The mass fractions of $Mg(OH)_2$ in surface-modified MFI particles were estimated by DSC and thermogravimetric analysis (TGA) performed on a Netzsch STA409. A sharp endothermic peak in the range of 370–430 °C appears in the DSC curve due to the dehydration of $Mg(OH)_2$ to MgO. The mass fraction of $Mg(OH)_2$ was calculated from the H_2O loss in this temperature region. The surface morphology and size of MFI crystals were determined using SEM (LEO 1530).

2.4.2. MFI/PVAc composites

Mechanical properties of polymer composite films were measured using a high-throughput impact and strain (HTMECH) apparatus. Details on the design and validation of this apparatus can be found elsewhere [27–29]. The films are contacted with a 1.5 mm diameter steel pin at a constant strain rate (0.5 mm/s), with the pin oriented normal to the film surface, resulting in equibiaxial deformation. Measurement points are isolated with a steel grid of 3 mm diameter holes at 4 mm spacing. A force sensor records the force–time profile for each of the 30 measurement points on a typical 2.5 × 2.0 cm^2 area of films. Each force–time profile was converted to strain–stress curve, and statistical mechanical properties of polymer composite films such as the tensile strength and elongation were obtained. All mechanical tests were performed under ambient conditions. To characterize the glass transition behavior of the composites, DSC measurements were performed with a TA instruments Q21 at a heating rate of 5 °C/min over the temperature range of −10–120 °C in a nitrogen atmosphere. Specimens about 4 mg for DSC measurements were cut out from the films prepared above and sealed in aluminum pans with lids. Onset temperatures at points where the glass transition begins and ends, respectively, were measured and the width of the glass transition, ΔT, was determined as a difference of each onset temperature. The glass transition temperature (T_g) was determined from the inflection point of the glass transition region of the samples which are annealed at 100 °C. The T_g

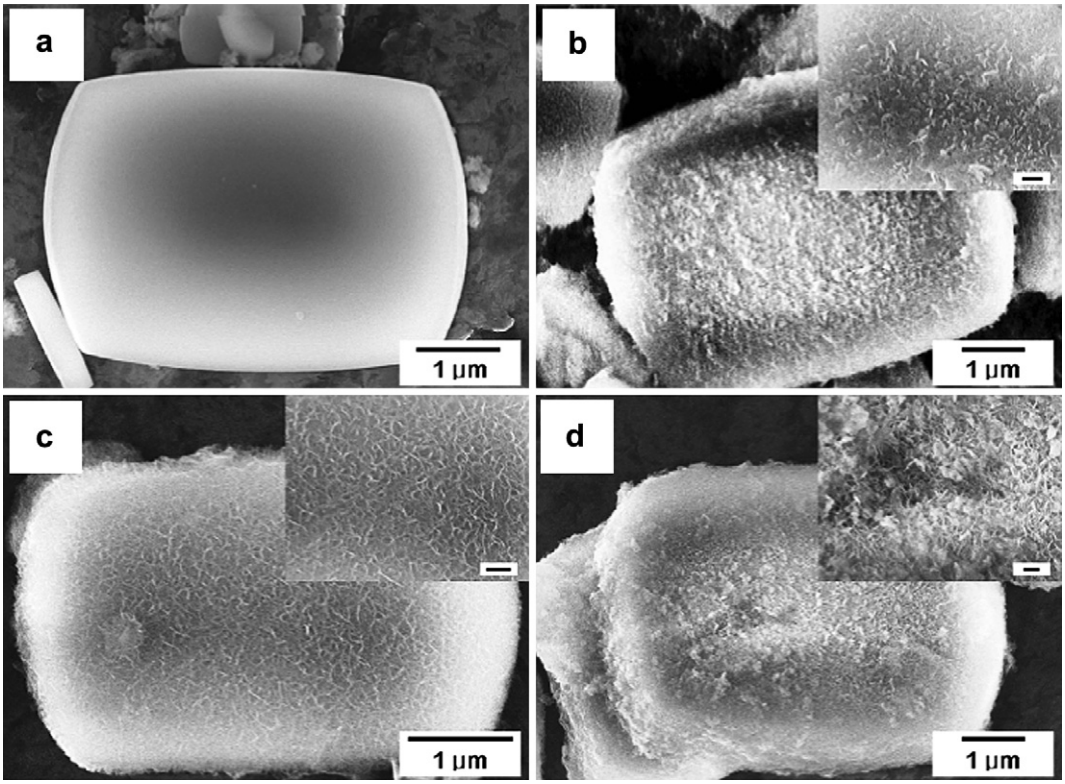

Fig. 2. MFI microparticles (μMFIs); (a) untreated (UN), (b) Grignard-treated (GT), (c) solvothermally-treated (ST), and (d) solvothermally-treated (HST, 20 wt% $Mg(OH)_2$).

value for pure PVAc was estimated to be around 45 °C [30]. All thermal properties of the samples were measured from the first heating run. Prepared composite films were also characterized by XRD. XRD patterns were obtained on a Philips X'pert Pro powder diffractometer and a PW3011 proportional detector equipped with a parallel plate collimator (CuKα, $\lambda = 1.5418$ Å). SEM was used to examine the interfacial morphology and particle dispersion of MFI/PVAc composites. Fracture surfaces of the composites containing 5 and 10 vol.% of untreated and surface-treated MFI were observed with a LEO 1530 instrument.

3. Results and discussion

3.1. Particle modification

The surface morphologies of untreated (UN) and surface-modified MFI nanoparticles (nMFIs) and microparticles (μMFIs), via Grignard (GT) or solvothermal treatment (ST), were compared using SEM images (Figs. 1 and 2).

Unmodified nMFIs show smooth surfaces, with a uniform "rounded-cubic" shape and size of around $300 \times 300 \times 150\ nm^3$ (see also Supporting information (Fig. S1a)). SEM images clearly show that the surface roughness of nMFI was significantly altered by GT or ST method, by the formation of inorganic whisker- or asperity-like nanostructures. The surface nanostructures were identified as $Mg(OH)_2$ by energy-dispersive spectroscopy (EDS) and XRD, as reported in a previous study [19]. The ST treatment produced well-defined nanowhiskers on the nMFI surfaces with higher surface roughness, compared to GT, which was further verified with external surface area analysis [19]. Since the surface roughness is strongly related with the surface external area, the surface roughness of the untreated and surface-modified MFI particles was quantified by BET (Brunauer–Emmett–Teller) external surface area previously [19], as illustrated in Table 1. The surface roughness of MFI particles increased significantly after GT and ST modifications, and ST-nMFI showed higher external surface area and hence higher surface roughness than GT-nMFI, which was consistent with SEM observations.

The length of the nanowhiskers created by ST method is estimated to be around 70 nm from the SEM images, as shown in Fig. 1c. Their width appears to be 1–2 orders of magnitude smaller than the length scale, indicating high aspect ratio structures. The mass fractions of $Mg(OH)_2$ of GT- and ST-nMFI samples were determined to be approximately 15 and 20 wt%, respectively from DSC and TGA measurements.

For the MFI microparticles (μMFIs), the untreated MFI crystals also have smooth surfaces with a "rounded-boat" shape, ranging in size from $1 \times 0.5 \times 0.2\ \mu m^3$ to $5 \times 3.5 \times 1\ \mu m^3$ with a broad size distribution as shown Fig. 2a (see also Supporting information (Fig. S1b)). After GT or ST modification, well-defined surface nanostructures were formed on the μMFI surface, which provide a large planar surface for the nucleation and growth of the nanostructures. The GT method created roughened surface morphologies composed of whisker- and platelet-shaped nanocrystals (Fig. 2b), while ST led to uniform whisker-like structures (~100 nm in length) with high aspect ratio (Fig. 2c). Similarly, the ST method resulted in higher surface roughness (higher external surface area), compared to GT, as shown in Table 1. The amount of $Mg(OH)_2$ in the GT- and ST-modified μMFIs was estimated to be around 5 wt%. ST-modified μMFIs with a higher amount of $Mg(OH)_2$ (~20 wt%) were also prepared, and these exhibit a denser nanowhisker morphology with increased roughness, compared to 5 wt% $Mg(OH)_2$ loaded samples (Fig. 2d).

Table 1
BET external surface area of untreated and surface-modified MFI particles [19].

	nMFI (m^2/g MFI)	μMFI (m^2/g MFI)
Untreated (UN)	7.5	3.7
Grignard-treated (GT)	39.8	11.0
Solvothermal-treated (ST)	74.5	35.1

3.2. MFI/PVAc composites

3.2.1. Morphology

The morphology of MFI–PVAc interfaces in composites was studied by examining SEM images of fracture surfaces. The interfaces in PVAc composites were influenced by the surface morphology (roughness) of MFI particles as well as annealing conditions of the films. Figs. 3 and 4 show SEM images of fracture surfaces of PVAc composites containing 10 vol.% of untreated and surface-modified particles for nMFI (Fig. 3) and μMFI (Fig. 4), respectively.

The films composed of PVAc and unmodified MFI particles, regardless of particle size, showed a dewetted filler–polymer interface with interfacial voids around the particles (Figs. 3a and 4a). The void-containing interfacial morphology of PVAc and untreated MFI is believed to be attributed in part to the intrinsically unfavorable interaction between the smooth MFI surface and the polymer phase. The interfacial voids seem to be reduced after melt annealing at 100 °C and subsequent slow cooling, which is apparent for the case of μMFIs (Fig. 4b).

The interfacial adhesion between the MFI surface and a series of polymer surfaces was measured in air using a zeolite colloidal probe AFM technique, as described previously [26]. It was found that adhesion forces between the zeolite and polymer surfaces were determined primarily by hydrogen bonding between the Lewis basic components of the polymer and acidic components on the zeolite. PVAc, containing the highest carbonyl group density compared to the polyimide and polyetherimide polymers examined, exhibited the strongest adhesion with MFI. The formation of interfacial voids at the MFI–PVAc interface observed in this study indicates that the interfacial attraction between MFI and PVAc is not sufficient to overcome other forces driving defect formation.

When the GT- or ST-modified MFI particles are incorporated into PVAc, the resultant films exhibited wetted PVAc–MFI interfaces with significantly reduced or no detectable interfacial voids (Fig. 3c and e, and Fig. 4c and e). The interfacial morphology of the composites is determined by the balance achieved between the PVAc–MFI interaction energy, the cohesive energy of the polymer, and the entropy changes associated with the available configurations. An entropic force drives the polymer chains away from the filler surface, while favorable interactions with the surface can potentially overcome these configurational limitations. Hence, the interplay of energetic and entropic factors determines the final structure of the composite. It has been proposed by others that nano-roughened structures may stabilize polymer chain adsorption at such interfaces, relative to flat surfaces, by minimizing entropic penalties for polymer adsorption [15,19,20,31,32]. The inorganic nanostructures on the modified MFI surface also greatly enlarge the contact area, so that any attractive interaction energy might be enhanced. This was illustrated by the result that the ST-nMFI, having a higher surface roughness, also showed further reduced interfacial voids than GT-nMFI (Fig. 3c and e), which was confirmed by DSC thermal analysis described below. We propose that both increased surface area and reduced entropic penalty for adsorption lead to the elimination of dewetted void morphologies in the surface-modified MFI/PVAc composites [15,19,20].

Likewise, the increased roughness of ST-MFI microparticles (μMFIs), induced by increasing the $Mg(OH)_2$ content from 5 to 20 wt %, may further enhance the compatibility of surface nanostructures

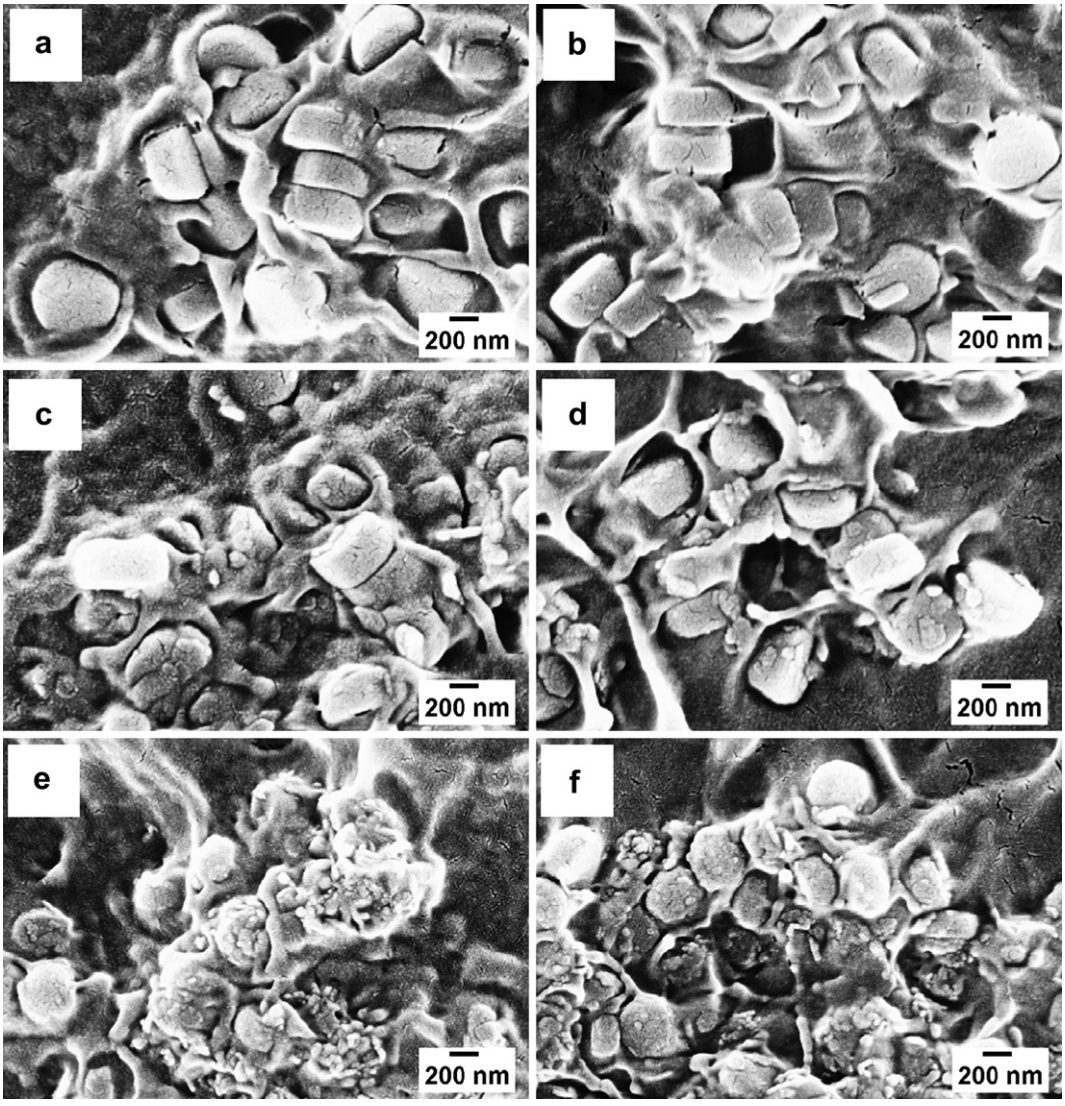

Fig. 3. SEM images of PVAc composites containing 10 vol.% of untreated and surface-treated MFI nanoparticles (nMFIs), which are annealed at 20 and 100 °C for 24 h, respectively: untreated (UN) (a) 20 °C and (b) 100 °C, Grignard-treated (GT, 15 wt% of $Mg(OH)_2$) (c) 20 °C and (d) 100 °C, and solvothermally-treated (ST, 20 wt% of $Mg(OH)_2$) (e) 20 °C and (f) 100 °C.

with the PVAc matrix. However, composites made with HST-μMFI containing 20 wt% of $Mg(OH)_2$ showed "naked" MFI particles and evidence of free whiskers in the film (Fig. 4g and h). This apparent delamination between the ST-deposited $Mg(OH)_2$ layer and the MFI surface may indicate relatively weak adhesion between the solid layer of 20 wt% of $Mg(OH)_2$ on the MFI surface, compared to the 5% $Mg(OH)_2$ sample. This result suggests that it is crucial to control the content of $Mg(OH)_2$ for achieving desirable interfacial morphology with minimal defects such as delamination and interfacial voids.

It is important to note that the degree of MFI particle (in particular nMFI) dispersion in the PVAc matrix was improved by surface modifications (GT and ST), which was clearly observed for higher MFI loading (≥5 vol.%), as shown in Fig. 5. The composites containing UN-nMFIs showed an inhomogeneous distribution of the particles with significant agglomerations in the composites, as indicated by arrows in Fig. 5a. On the other hand, surface-treated (GT and ST) nMFIs were more homogeneously dispersed in the PVAc matrix with a lower tendency to form agglomerates (Fig. 5b and c). It is known that the improved particle–polymer interfacial adhesion facilitates particle dispersion in the composites [1,33]. The relatively better dispersion of GT- and ST-nMFIs in the PVAc matrix further confirms the improved interfacial adhesion between the MFI surface and the PVAc matrix by surface modifications.

The interfacial morphology of composites depends on the annealing temperature as well as the surface roughness of the filler. Annealing at high temperature (100 °C), above the T_g of PVAc, reduced the size of interfacial voids in the PVAc composites made with untreated MFI particles, which is clearly observed for the case of microparticles (Fig. 4b). Annealing provides additional mobility to PVAc chain segments, which likely enables access to otherwise inaccessible regions around the zeolites, results in relaxation of void defects near the MFI–matrix interface [14]. Another possible mechanism for the observed reduction in interface voids after annealing above T_g is that air bubbles existing in the void region might become mobile and could diffuse out through PVAc during the annealing process. However, high temperature annealing induced interfacial voids in PVAc composites embedded with GT- or ST-nMFI, as shown in Fig. 3d and f. Because these voids are associated with the apparent stripping of whiskers from the nMFI surface, the increased voids are likely explained by a relatively weaker adhesion of surface nanostructures with the nMFI surface, compared to that with the PVAc matrix. PVAc chain relaxation

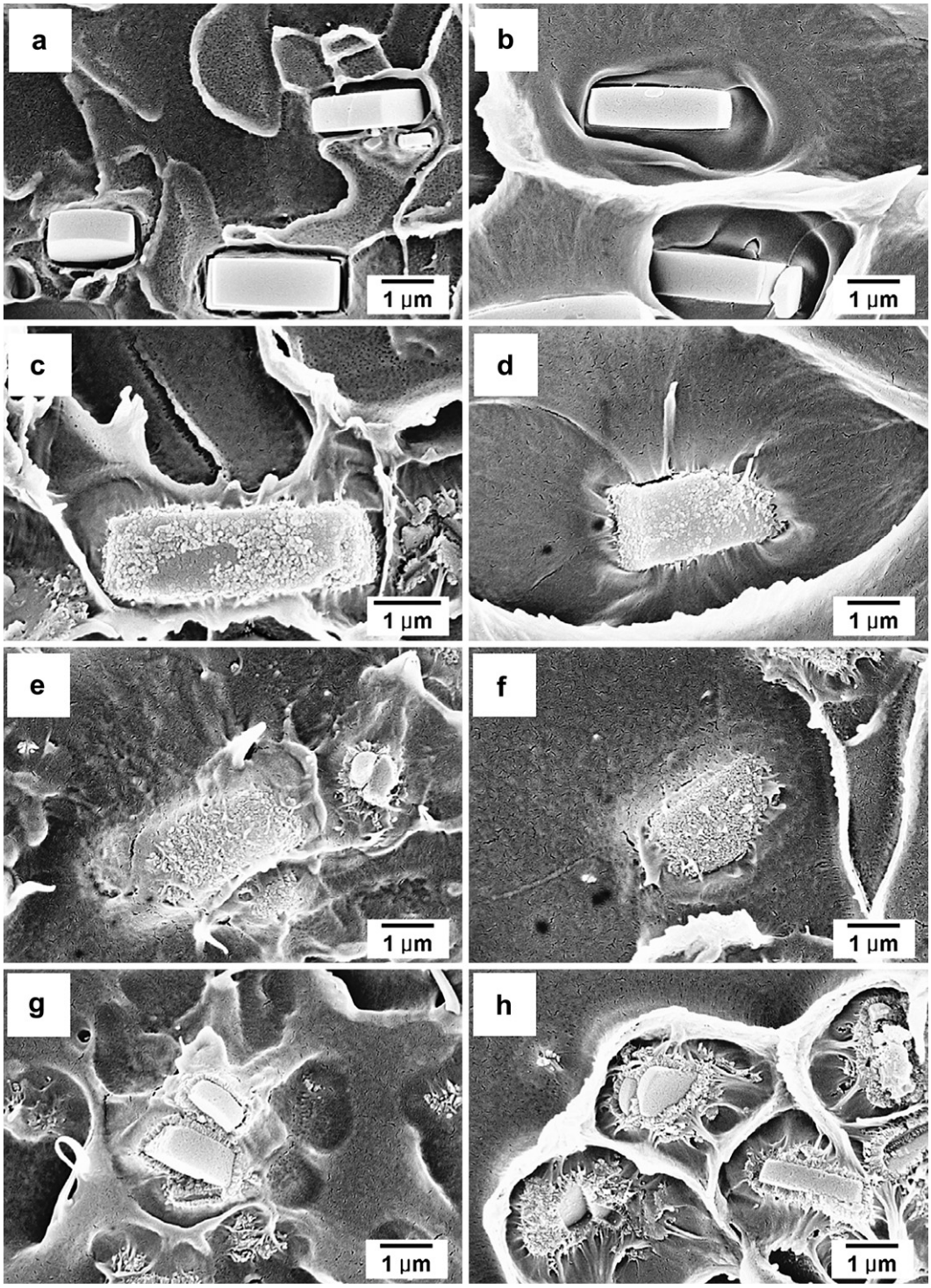

Fig. 4. SEM images of PVAc composites containing 10 vol.% of untreated and surface-treated MFI microparticles (μMFIs), which are annealed at 20 and 100 °C for 24 h, respectively: untreated (UN) (a) 20 °C and (b) 100 °C, Grignard-treated (GT, 5 wt% of $Mg(OH)_2$) (c) 20 °C and (d) 100 °C, solvothermally-treated (ST, 5 wt% of $Mg(OH)_2$) (e) 20 °C and (f) 100 °C, and solvothermally-treated (HST, 20 wt% $Mg(OH)_2$) (g) 20 °C and (h) 100 °C.

during melting and subsequent slow cooling likely produces stress at the polymer–particle interface, resulting in delamination between the whisker structures and the nMFI surface with increased interfacial voids (Fig. 3d and f).

Contrary to nMFI, nano-roughened structures on the μMFI surface still exhibited the wetted particle–PVAc interface even after melt annealing, shown in Fig. 4d and f. This robust improvement in interfacial morphology after annealing is additional evidence of that $Mg(OH)_2$ nanostructures are more strongly adhered to μMFI surfaces than nMFI. Considering that the nanostructure dimensions are near 40–100 nm, the reduced curvature of the μMFI particle planar surfaces may result in more stable nucleation and growth of the nanostructures than nMFI with higher curvature [19]. Hence, the formation of stably-bound nanostructures with significant strength to withstand residual stress during composite annealing can be achieved on the larger μMFI particles.

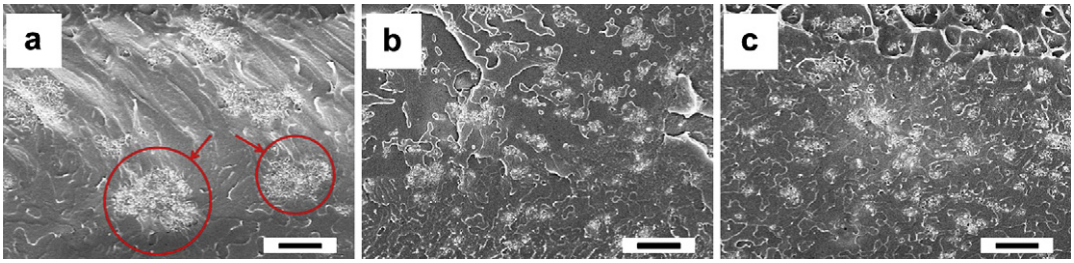

Fig. 5. SEM images of PVAc composites containing 5 vol.% of (a) untreated (UN), (b) Grignard-treated (GT), and (c) solvothermally-treated (ST) MFI nanoparticles (nMFIs). The scale bars indicate 5 μm.

In a previous study [26] we measured the interaction force between PVAc and polyimides with μMFI, and found that the interaction force was governed by a combination of van der Waals and acid–base interaction forces. In particular, that previous study revealed the importance of –C=O groups serving as electron donors (Lewis bases) for interactions with acid-containing surfaces like zeolites. In the case of untreated μMFI the particle–polymer interfacial attraction was 210 ± 10 ($\times 10^3$ N/m^2), which increased to 630 ± 40 N/m^2 for GT-modified zeolite-MFI. Hence, the increased adhesion strength in GT-MFI, measured independently, is consistent with the observed improvement in wetting from the present paper. It is interesting to note that the increase in adhesion strength was similar in magnitude to the 3× increase in surface area achieved after GT modification (Table 1 above). This 3× improved interfacial adhesion by surface modification (GT and ST) apparently is sufficient to reduce interfacial-void defect formation.

3.2.2. Mechanical properties

Mechanical characterization of MFI/PVAc composites was performed to determine how mechanical properties were influenced by the presence of untreated or surface-modified MFI particles. Representative tensile stress–strain curves for pure PVAc and PVAc composites containing 10 vol.% of unmodified μMFIs at different annealing temperatures are presented in Fig. 6.

The addition of MFI particles led to a decrease in both the tensile strength and elongation at break. The modulus of PVAc composites is indistinguishable from that of pure PVAc up to strains of ~10%. Even

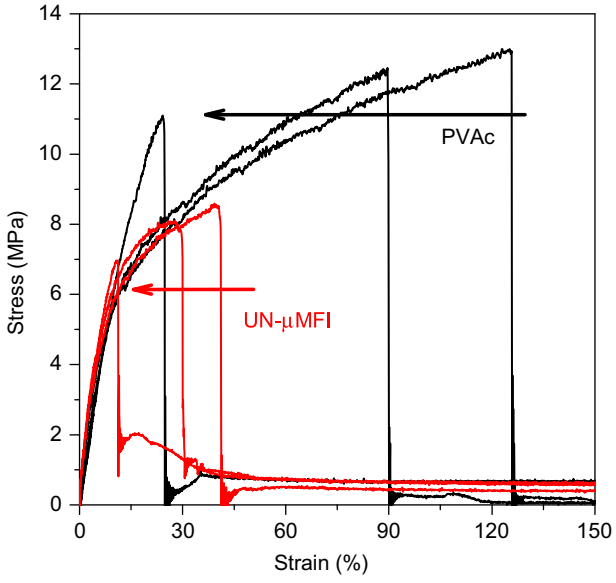

Fig. 6. Stress–strain curves for pure PVAc and PVAc composites containing 10 vol.% of untreated MFI microparticles (UN-μMFIs), annealed at 20, 40 and 100 °C for 24 h, respectively. (Annealing temperature increases along the arrow).

in the absence of filler, the mechanical properties of polymer may change during annealing [34]. In particular, the elongation at break significantly decreased with increasing annealing temperature for both pure PVAc and PVAc composites. This indicates that the PVAc matrix becomes more brittle as annealing temperature increases, in keeping with known densification behavior of amorphous glassy polymers annealed above T_g.

The tensile strength and elongation at break of PVAc composites containing untreated and surface-treated nMFI or μMFI particles, as a function of filler loading (0–10 vol.%) and annealing temperatures (20 and 100 °C) are shown in Figs. 7 and 8, respectively. For the PVAc composites annealed at 20 °C, both the tensile strength and elongation slightly increased with MFI loading up to 1 vol.% MFI and decreased beyond that, regardless of the size and surface morphology of MFI particles. The tensile strength and elongation of the composites depends strongly on the effectiveness of stress transfer and the fracture behavior associated with stress concentration at the filler–matrix interfaces [1,21,35]. This decrease in mechanical properties with increasing MFI content can be explained by poor interfacial adhesion and hence inefficient stress transfer between the filler surface and the polymer matrix, which was verified with void formation around the filler surface observed in SEM images (Figs. 3a,b and 4a,b) [1,21].

For a given particle volume fraction, the mechanical properties of the composites further decreased for the smaller nMFIs. This is attributed to the increased polymer–MFI interfacial area which was proven to be inefficient at transferring stress. Although both the tensile strength and elongation at break decreased with MFI loading, the reduction in the mechanical properties of PVAc composites was suppressed via GT or ST modification on the MFI particles (Figs. 7a and 8a). At 10 vol.% of GT-MFI or ST-MFI enhanced tensile strength and elongation at break were clearly observed relative to UN-MFI/PVAc composites, suggesting improved interfacial adhesion due to surface modification of the particles with nanowhisker structures [1]. Improved adhesion and hence reduced defect formation at polymer–particle interfaces and improved particle dispersion (in particular for nMFIs) is known to enhance the effectiveness of load transfer and minimize stress concentration at the particle–polymer interface or between particles, leading in an increase in strength and elongation [21,35,36]. Together with SEM evidence, the mechanical enhancement of composites made with surface-treated MFI, relative to untreated MFI, results from improved interfacial adhesion with minimal interfacial voids and better particle dispersion (for nMFIs) associated with nano-roughened structures on the particle surfaces (Figs. 3, 4 and 5). Shu et al. suggested that the physical roughness of nanowhisker structures on LTA zeolite particle surfaces enhances their interfacial adhesion with Ultem® poly(etherimide) and thus improves mechanical properties of resultant composites [15]. Thermodynamically-induced adsorption (smaller entropy loss upon adsorption) and increased attractive interaction by enlarged contact area are proposed to be possible reasons for enhancement in interfacial

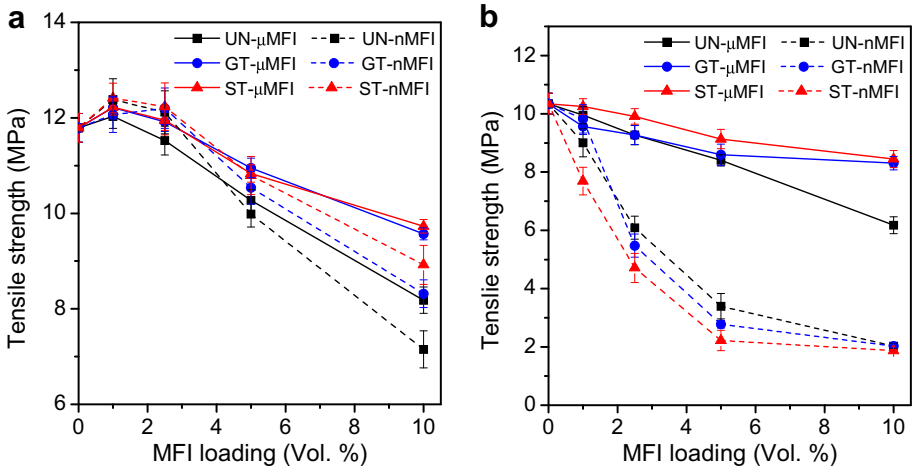

Fig. 7. Tensile strength of PVAc composites containing untreated (UN), Grignard-treated (GT), and solvothermally-treated (ST) MFI nanoparticles (nMFIs, dash line) or microparticles (μMFIs, solid line) as a function of MFI loading (1–10 vol.%) and annealing conditions ((a) 20 °C and (b) 100 °C for 24 h, respectively).

adhesion at the particle–polymer interface by creating nano-asperities on the particle surface [15,19,20].

The mechanical behavior of the composite films strongly relies on the annealing temperature. For the samples annealed at 100 °C, both the mechanical strength and elongation show a monotonic decrease as MFI loading increases (Figs. 7b and 8b) for all cases. The reduction of mechanical properties by addition of MFI particles to the polymer matrix was most significant for the smaller nMFI particles having a higher total surface area [21]. This result implies that the interfacial stress transfer between the MFI surface and the polymer phase is still inefficient after melt annealing. Although interfacial voids were reduced after higher temperature annealing, voids still existed as shown Figs. 3b and 4b. Thus, the particle cannot transfer any load and the mechanical properties of the composite decrease with increasing particle loading.

The effects of annealing temperature on the mechanical properties of the composites containing 10 vol.% of MFI particles are shown in Fig. 9. The elongation for both pure PVAc and PVAc composite films significantly decreased at higher temperature annealing, since the PVAc matrix becomes brittle with increased extent of chain relaxation. After annealing at lower temperature (20 °C), PVAc films filled with 10 vol.% of surface-modified MFI particles showed higher mechanical properties than composites with unmodified MFI, regardless of particle size. However, mechanical enhancement by nanostructured nMFIs decreased with increasing annealing temperature, and finally, no improvement was observed for samples annealed at 100 °C. On the contrary, the films containing nano-structured μMFIs exhibited mechanical enhancement over the untreated MFI samples over the entire range of annealing temperature, indicating the formation of strongly-bound nanostructures on the larger MFI surface. This result correlates well with the interfacial morphology observed from SEM images, where the nanostructured nMFIs induced interfacial voids, while nanostructured μMFI surfaces suppressed the formation of interfacial voids after annealing at high temperature (100 °C). Therefore, the creation of nanoscale morphology on the MFI surface, in particular on μMFIs, is correlated strongly with improved interfacial adhesion, minimal void formation, and improved mechanical properties compared to unmodified MFI. This is likely mediated by improved load transfer between the zeolite and the polymer matrix. The robust effect of nanostructured μMFIs, and the absence of these improvements with nanostructured nMFI, is probably attributed to relatively strongly-adhered nano-asperities on the larger particle, as discussed above.

Interestingly, the film containing ST-μMFI with a higher content (20 wt%) of $Mg(OH)_2$ showed significantly reduced mechanical properties with increasing annealing temperature, with strength and elongation falling below even those of bare MFI filled samples. The poor mechanical properties are correlated with observed

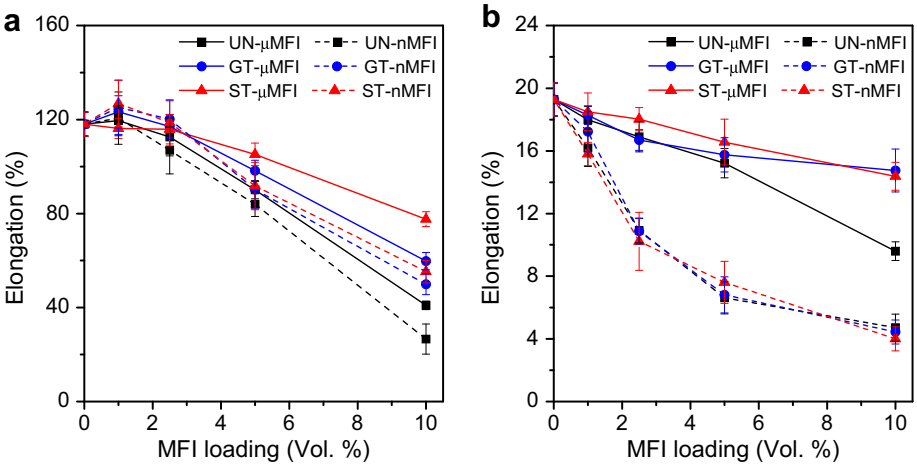

Fig. 8. Elongation at break of PVAc composites containing untreated (UN), Grignard-treated (GT), and solvothermally-treated (ST) MFI nanoparticles (nMFIs, dash line) or microparticles (μMFIs, solid line) as a function of MFI loading (1–10 vol.%) and annealing conditions ((a) 20 °C and (b) 100 °C for 24 h, respectively).

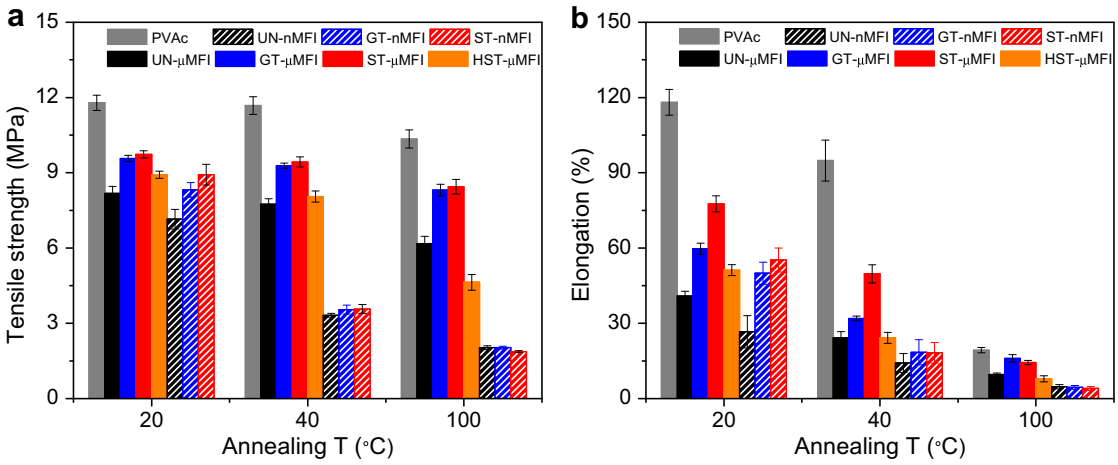

Fig. 9. Mechanical properties (a) tensile strength and (b) elongation at break of pure PVAc and PVAc composites containing 10 vol.% of untreated (UN), Grignard-treated (GT), and solvothermally-treated (ST) MFI nanoparticles (nMFIs) or microparticles (μMFIs) as a function of annealing temperatures (20, 40, and 100 °C for 24 h, respectively). HST denotes solvothermal treatment with a higher content (20 wt%) of $Mg(OH)_2$.

delamination between the nanowhiskers and the zeolite surface, and free whiskers dispersed in the PVAc matrix (Fig. 4g and h). Relaxation of the polymer phase with increased annealing temperature is likely to further pull the nanostructures away from the particle surface and hence increase the degree of delamination (void) acting as stress concentration region, leading to a decrease in stress transfer efficiency. In addition to this delamination factor, undesirable free whiskers might further decrease mechanical properties by creating additional inorganic–polymer interfaces which are not efficient for stress transfer.

3.2.3. Thermal properties

When an amorphous polymer is cooled from the rubbery to the glassy state through the glass transition region, the polymer below the T_g is in a non-equilibrium state characterized by excess volume, entropy, enthalpy and internal stress [34,37–40]. The polymer slowly approaches the thermodynamic and structural equilibrium state through the conformational rearrangement of polymer segments under isothermal conditions. This process towards equilibrium is referred to as annealing, physical aging, or relaxation, and its rate depends on the physical environment (structural mobility) of the glass and the annealing temperature [37,38,40]. Increasing chain mobility or annealing temperature, close to but below the T_g of the polymer, accelerates the relaxation rate. The polymer structure is densified and becomes more uniform, as it moves to a more nearly equilibrium state upon annealing [39].

The thermal behavior of composite materials reflects the relaxation characteristics of polymer at the particle interface as well as that of the bulk polymer [23]. To better understand how the incorporation of nanostructured MFI affects the glass transition behavior associated with enthalpic relaxation, DSC measurements were performed on the composites with respect to the surface morphology of the fillers and annealing temperature. The widths of the glass transition, ΔT, as determined by difference between the starting and the ending points of the glass transition region, for all specimens after annealing at different temperatures were listed in Table 2. The T_g values were determined from DSC spectra of the samples annealed at 100 °C. Representative DSC spectra and ΔT values for pure PVAc and PVAc composites containing 10 vol.% of nMFIs with different surface treatments, as a function of annealing temperatures, are presented in Fig. 10.

The neat PVAc is purely amorphous without any melting peak in the DSC curves. The changes in the glass transition with increased annealing temperature showed similar trends for both pure PVAc and PVAc composites: broad endothermic peaks appeared in the DSC heating curve of the samples annealed at 20 °C, attributed to a broad distribution of different relaxation times associated with a wide distribution of molecular environments having different conformational mobilities [24,30,38]. The position, magnitude and broadness of the peak is an indirect measure of the extent of enthalpic relaxation during annealing [38]. The endothermic peak shifts to higher temperature, increases in height, and narrows with increased annealing temperature. Theses changes in the glass transition peak are usually understood to be due to homogenization of chain segment local environments during the annealing process [38,41].

MFI/PVAc composites showed a narrower glass transition region than that of neat PVAc when the samples were annealed below T_g (20 and 40 °C), in particular for UN-nMFI/PVAc composites. This characteristic glass transition behavior of UN-nMFI/PVAc composites was similar with the case of larger sized μMFI, where the narrow and intense transition of UN-μMFI/PVAc composite was observed in the sub-T_g annealed samples (see Supporting information (Fig. S2)). On the other hand, no significant differences in the breadth or T_g value was observed between neat PVAc and PVAc composites after melt annealing at 100 °C for either nMFI or μMFI, as illustrated in Table 2.

In polymer composites, the presence of fillers can significantly influence the relaxation dynamics and glass transition behavior of the polymer by altering the local structure near the filler interface

Table 2
Thermal properties (the width of the glass transition, ΔT, and T_g) of pure PVAc and PVAc composites containing 10 vol.% of untreated (UN), Grignard-treated (GT), and solvothermally-treated (ST) MFI nanoparticles (nMFIs) or microparticles (μMFIs) as a function of annealing temperatures (20, 40, and 100 °C for 24 h, respectively).

Samples	ΔT (°C)			T_g (°C)
	20 °C	40 °C	100 °C	
Pure PVAc	23.6 ± 0.9	15.5 ± 0.7	5.1 ± 0.6	44.9 ± 2.2
UN-nMFI	15.4 ± 1.3	10.5 ± 0.5	4.3 ± 0.5	44.7 ± 1.9
GT-nMFI	20.0 ± 1.2	12.7 ± 0.6	4.4 ± 0.2	45.5 ± 2.2
ST-nMFI	22.4 ± 1.7	14.8 ± 1.1	4.0 ± 0.4	45.7 ± 1.1
UN-μMFI	14.7 ± 1.9	–	4.1 ± 0.3	44.6 ± 0.5
GT-μMFI	20.6 ± 1.2	–	4.3 ± 0.2	45.9 ± 1.3
ST-μMFI	22.9 ± 1.1	–	4.3 ± 0.6	43.9 ± 0.9

Note. Uncertainty is standard deviation.

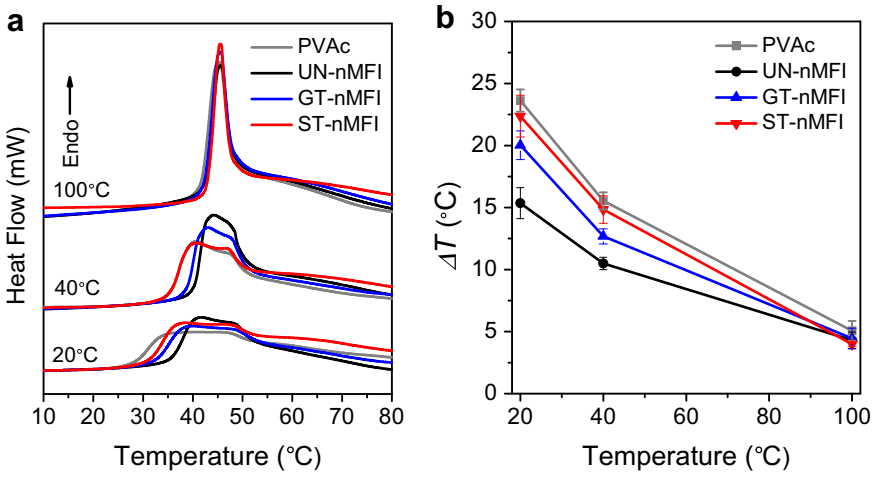

Fig. 10. (a) DSC curves and (b) the width of the glass transition (ΔT) of pure PVAc and PVAc composites containing 10 vol.% of untreated (UN), Grignard-treated (GT), and solvothermally-treated (ST) MFI nanoparticles (nMFIs) as a function of annealing temperatures (20, 40, and 100 °C for 24 h, respectively).

[22,23,37]. The width of the thermal transition and T_g value in DSC curves was known to be altered with the addition of fillers, depending on the level of the polymer–filler interactions at interface [23,37,38,42,43]. The chain relaxation dynamics of the filled systems can be suppressed or accelerated in comparison with the neat polymer by changing the mobility of polymer segments in the vicinity of the filler interface, depending on the strength of attractive interaction between the polymer and the filler [23,37,42]. If the polymer chains have a strong affinity for the particle surface, strongly-bound polymer chains near the filler surface experience a reduction in the chain mobility [22,23,37–40,42,44–46]. This restriction effect retards the rate of segmental relaxation relative to that of the neat polymer, and increases the T_g [22,23,37,40,42,43]. In addition, the relaxation dynamics can determine the breadth of the relaxation time distribution [37]. In fact, a strong interaction between polymer and filler tends to broaden the glass transition of composites compared to that of bulk polymers [23,37,40,42,46].

Alternatively, if there are voids present around the filler particle, then the polymer exists in a state similar to a polymer–air interface. Although MFI exhibited higher adhesion with PVAc than with polyimide and polyetherimide, the MFI–PVAc interfacial adhesion is apparently not strong enough to prevent void formation as mentioned above. The weakness of the MFI–PVAc interactions is evident in SEM observation of composite fracture surfaces where the dewetted interface between the untreated MFI surface and the PVAc, with large interfacial voids around fillers was apparent (Figs. 3a and 4a). Hence, in the MFI/PVAc composites, there is an effective air–polymer interface around each particle. The free surface is characterized as a highly mobile liquid-like interface having lower activation energy for conformational chain rearrangement and a narrower distribution of relaxation times than those of bulk polymer [45,47]. This enhanced mobility is hypothesized to be mainly due to the segregation of chain ends to the free surface due to conformational entropy. The relaxation rate of chain segments in free surfaces is much faster than that of bulk polymer [45]. Hence, two relaxation domains with different relaxation rates can be proposed to exist in the MFI/PVAc composite system: the modes corresponding to the normal segmental motion of bulk polymer and faster relaxation dynamics corresponding to more mobile segments in the air/polymer interface in internal voids. Since the overall relaxation behavior of polymer composites depends on the relative contributions of the dynamics of each domain, the presence of a poorly-interacting filler increases the overall relaxation rate by creating highly mobile polymer regions around particles. Thus, under the same annealing condition the polymer matrix in the PVAc composite containing untreated MFI particles approaches the equilibrium glass state further, resulting in narrowing in width and increasing in the height of glass transition region, comparing to bulk PVAc. On the other hand, the PVAc composites prepared with surface-modified (GT or ST) particles showed relatively broader glass transition peaks than composites with untreated particles. The broader glass transition in surface-modified MFI composites is consistent with the wetted PVAc–filler interfaces observed in SEM images. The observed difference in the width of the DSC endothermic peak of MFI/PVAc composites seems to depend on the degree (size and fraction) of interfacial voids surrounding the particles: the higher degree of interfacial voids (poorly wetted interface) for untreated MFI resulted in narrower and higher peaks due to the increased rate and extent of relaxation caused by enhancing overall chain mobility. On the other hand, improved polymer–filler interaction and hence suppressed formation of interfacial voids observed in surface-modified MFI fillers is responsible for the relatively broader glass transition region observed in those samples. ST-nMFI, with a smaller degree of interfacial voids, showed broader and weaker glass transition peaks than GT-nMFI, as presented in Fig. 10 and Table 2. This result supports the idea that the more roughened surface created by ST treatment is more effective in enhancing interaction with PVAc, compared to the GT treatment. Surface-treated samples, however, still showed narrower glass transitions than that of neat PVAc after sub-T_g annealing. This implies that the interfacial voids might not be completely removed even though they are significantly reduced by surface modification.

In addition, the T_g of samples annealed at 100 °C were compared and there was no detectable difference in the value of T_g between pure PVAc and PVAc composites, within measurement error. These results suggest that the interaction between the highly relaxed PVAc matrix and either the bare or surface-modified particle is not strong enough to shift the overall T_g of the composite.

3.2.4. XRD characterization

Pure PVAc and PVAc composite films composed of MFI particles with different surface morphology were subjected to XRD to obtain further information regarding the interaction of zeolite particles with the polymer matrix. Fig. 11a depicts the XRD patterns of pure PVAc and PVAc composites containing untreated μMFIs annealed at 20 °C and 100 °C. The XRD patterns of pure PVAc films annealed at

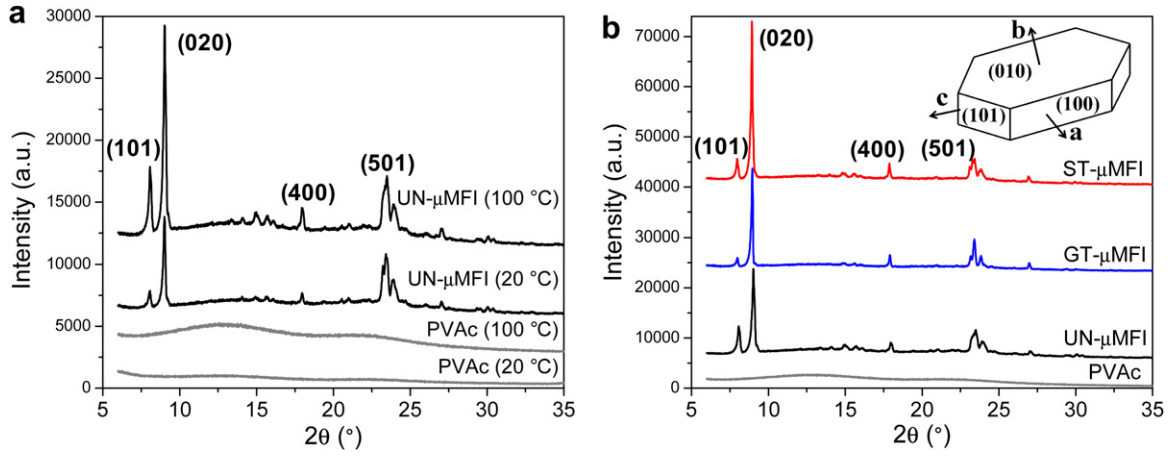

Fig. 11. XRD patterns of (a) pure PVAc and PVAc composite films containing 10 vol.% of untreated (UN) MFI microparticles (μMFIs), which are annealed at 20 and 100 °C for 24 h, respectively, (b) pure PVAc and PVAc composite films composed of 10 vol.% of untreated, Grignard-treated (GT), and solvothermally-treated (ST) μMFIs after annealing at 100 °C for 24 h.

20 °C display two broad peaks at 13.1° and 22.1°, being consistent with those reported previously [48,49]. These broad peaks result from the amorphous nature of PVAc and become more pronounced after annealing at 100 °C, implying that significant chain relaxation has occurred after melt annealing followed by slow cooling. For the MFI/PVAc composites, the presence of μMFIs within the PVAc matrix can be identified by a series of characteristic peaks around 8.2°, 9.1°, and 23.5°, which can be indexed as (101), (020) and (501) planes, respectively. For the unmodified μMFI, the relative intensities of these characteristic peaks remained essentially unchanged after annealing at 100 °C.

On the other hand, interestingly, it was observed that intensity of the (020) MFI refraction was preferentially intensified after annealing at 100 °C for composites filled with surface-modified μMFI, as presented in Fig. 11b. The relative (020) peak intensity is more pronounced, relative to the (101) peak, for the films made with GT- or ST-μMFIs, compared to the (020) peak of untreated MFI composites. This result indicates that the surface-modified MFI particles are oriented preferentially with the b-out-of-plane direction within the PVAc matrix. This orientation preference may be attributed to the improvement in affinity of MFI filler with the PVAc phase associated with inorganic nanostructures on the filler surface, as illustrated in the morphological, mechanical and thermal characterization of the composites above. The rearrangement of polymer chain segments during the annealing process may favor a specific orientation of the surface-treated MFI crystals that has more favorable interactions with the PVAc matrix. This result suggests that, by appropriate selection of the surface treatment method and the composite fabrication protocol, MFI particles with surface nanowhiskers may present a preferred orientation in the matrix, which often becomes critical to the film performance such as mechanical and membrane properties [50,51].

4. Conclusions

In this study, the effect of MFI zeolite loading, size, and surface treatment (Grignard or solvothermal method) with $Mg(OH)_2$ inorganic nanowhiskers on the structural, mechanical and thermal properties of MFI/PVAc composites was investigated. The ST method produced well-defined nanowhiskers on MFI surfaces with higher surface roughness, compared to the GT method. It was found that the presence of nanostructures on the MFI surface improves compatibility and interfacial adhesion between the zeolite and the polymer matrix, resulting in nearly defect-free interfaces and better particle dispersion (especially for MFI nanoparticles) in the composites. This enhancement is attributed to surface roughening that facilitates adsorption on the nanowhisker structures. This surface roughening effect was further confirmed by the fact that increased surface roughness in the ST-MFI sample results in more interfacial enhancement than the GT-MFI sample. The mechanical characterization reveals that PVAc composites containing surface-modified particles have higher mechanical strength than those embedded with unmodified MFIs at the same MFI loading. The annealing temperature of the composites has a strong influence on the morphological and mechanical properties of the films. The mechanical and morphological enhancement by surface modifications on the MFI nanoparticles decreased with increasing annealing temperature, while surface-modified MFI microparticles exhibited improvements relative to untreated samples over a wide range of annealing temperature. This robust effect of the nanostructured microparticles indicates the formation of strongly-adhered nanostructures on the larger MFI surface. The improved mechanical properties and interfacial morphology were also observed to be dependent on the amount of $Mg(OH)_2$ present on the surface of GT-μMFI. The dewetted (air/polymer) interfaces (interfacial voids) observed for untreated MFI composites resulted in narrow glass transition regions due to the increased rate and extent of relaxation caused by high mobility of the polymer segments around the filler. On the contrary, the improved wetted interface (suppressed formation of interfacial voids) observed for surface-modified MFI fillers, led to slower relaxation and a broader glass transition region compared to that of unmodified particles. However, the extent of adhesion of the nanostructured MFI surface with the PVAc phase is apparently not strong enough to broaden the width and increase T_g value of PVAc by chain restriction effects. Improved interactions between the polymer and the surface-modified MFI particles induced a preferential orientation of the MFI particles within the PVAc matrix during annealing process, confirmed by XRD analysis.

Acknowledgements

We are grateful to the ExxonMobil company for support of this research. Special appreciation is extended to Tae-Hyun Bae, Dr. Sankar Nair and Dr. Christopher Jones for the provision of facilities for synthesis and modification of MFI zeolite, and Dr. Bill Koros for providing polymers used herein.

Appendix. Supporting information

Supporting information (SEM images of MFI particles and DSC curves of μMFI/PVAc composites) associated with this article can be found, in the online version, at doi:10.1016/j.polymer.2010.09.071.

References

[1] Metin D, Tihminhoglu F, Balkose D, Ulku S. Composites Part A 2004;35(1):23–32.
[2] Beecroft LL, Ober CK. Chem Mater 1997;9(6):1302–17.
[3] Molenkamp WC, Watanabe M, Miyata H, Tolbert SH. J Am Chem Soc 2004;126(14):4476–7.
[4] Libby B, Smyrl WH, Cussler EL. AIChE J 2003;49(4):991–1001.
[5] Quaglia M, De Lorenzi E, Sulitzky C, Caccialanza G, Sellergren B. Electrophoresis 2003;24(6):952–7.
[6] Clark JH, Macquarrie DJ. Chem Commun 1998;(8):853–60.
[7] Wight AP, Davis ME. Chem Rev 2002;102(10):3589–614.
[8] Jeong HK, Nair S, Vogt T, Dickinson LC, Tsapatsis M. Nat Mater 2003;2(1):53–8.
[9] Robeson LM. J Memb Sci 1991;62(2):165–85.
[10] Chung TS, Jiang LY, Li Y, Kulprathipanja S. Prog Polym Sci 2007;32(4):483–507.
[11] Li Y, Guan HM, Chung TS, Kulprathipanja S. J Membr Sci 2006;275(1–2):17–28.
[12] Husain S, Koros WJ. J Membr Sci 2007;288(1–2):195–207.
[13] Mahajan R, Burns R, Schaeffer M, Koros WJ. J Appl Polym Sci 2002;86(4):881–90.
[14] Mahajan R, Koros WJ. Ind Eng Chem Res 2000;39(8):2692–6.
[15] Shu S, Husain S, Koros WJ. J Phys Chem C 2007;111(2):652–7.
[16] Pechar TW, Tsapatsis M, Marand E, Davis R. Desalination 2002;146(1–3):3–9.
[17] Singh A, Koros WJ. Ind Eng Chem Res 1996;35(4):1231–4.
[18] Vankelecom IFJ, VandenBroeck S, Merckx E, Geerts H, Grobet P, Uytterhoeven JB. J Phys Chem 1996;100(9):3753–8.
[19] Bae TH, Liu JQ, Lee JS, Koros WJ, Jones CW, Nair S. J Am Chem Soc 2009;131(41):14662–3.
[20] Liu JQ, Bae TH, Qiu WL, Husain S, Nair S, Jones CW, et al. J Membr Sci 2009;343(1–2):157–63.
[21] Fu SY, Feng XQ, Lauke B, Mai YW. Composites Part B 2008;39(6):933–61.
[22] Amanuel S, Gaudette AN, Sternstein SS. J Polym Sci Part B Polym Phys 2008;46(24):2733–40.
[23] Arrighi V, McEwen IJ, Qian H, Prieto MBS. Polymer 2003;44(20):6259–66.
[24] Hutchinson JM. Thermochim Acta 1998;324(1–2):165–74.
[25] Verma SK, Bisarya SC. J Appl Polym Sci 1986;31(8):2675–84.
[26] Lee JH, Thio BJR, Bae TH, Meredith JC. Langmuir 2009;25(16):9101–7.
[27] Sormana JL, Meredith JC. Macromolecules 2004;37(6):2186–95.
[28] Sormana JL, Meredith JC. Mater Res Innov 2003;7(5):295–301.
[29] Sormana JL, Meredith JC. Macromol Rapid Commun 2003;24(1):118–22.
[30] Wu WB, Chiu WY, Liau WB. J Appl Polym Sci 1997;64(3):411–21.
[31] Baumgartner A, Muthukumar M. J Chem Phys 1991;94(5):4062–70.
[32] Douglas JF. Macromolecules 1989;22(9):3707–16.
[33] Ray SS, Okamoto M. Prog Polym Sci 2003;28(11):1539–641.
[34] Sung CSP, Lamarre L, Chung KH. Macromolecules 1981;14(6):1839–41.
[35] Ahmad FN, Jaafar M, Palaniandy S, Azizli KAM. Composite Sci Technol 2008;68(2):346–53.
[36] Kovacevic V, Packham D, Lucic S, Hace D, Smit I. Polym Eng Sci 1999;39(8):1433–43.
[37] Lu HB, Nutt S. Macromolecules 2003;36(11):4010–6.
[38] Alves NM, Mano JF, Balaguer E, Duenas JMM, Ribelles JLG. Polymer 2002;43(15):4111–22.
[39] Yoshida H. Thermochim Acta 1995;266:119–27.
[40] Salehi-Khojin A, Jana S, Zhong WHK. J Mater Sci 2007;42(15):6093–101.
[41] Liao KR, Quan DP, Lu ZJ. Eur Polym J 2002;38(1):157–62.
[42] Rittigstein P, Torkelson JM. J Polym Sci Part B Polym Phys 2006;44(20):2935–43.
[43] Yim A, Chahal RS, Stpierre LE. J Colloid Interface Sci 1973;43(3):583–90.
[44] Tsagaropoulos G, Eisenberg A. Macromolecules 1995;28(1):396–8.
[45] Ash BJ, Siegel RW, Schadler LS. J Polym Sci Part B Polym Phys 2004;42(23):4371–83.
[46] Verghese KNE, Jensen RE, Lesko JJ, Ward TC. Polymer 2001;42(4):1633–45.
[47] Ash BJ, Rogers DF, Wiegand CJ, Schadler LS, Siegel RW, Benicewicz BC, et al. Polym Compos 2002;23(6):1014–25.
[48] Elashmawi IS, Hakeem NA, Abdelrazek EM. Physica B 2008;403(19–20):3547–52.
[49] Zidan HM. J Polym Sci Part B Polym Phys 2003;41(1):112–9.
[50] Bonilla G, Vlachos DG, Tsapatsis M. Microporous Mesoporous Mater 2001;42(2–3):191–203.
[51] Chau JLH, Wan YSS, Gavriilidis A, Yeung KL. Chem Eng J 2002;88(1–3):187–200.